Materials Transactions, Vol. 50, No. 9 (2009) pp. 2221 to 2228

Mechanical Properties of Dense Cordierite Discs Sintered by Solar Radiation Heating

Fernando Almeida Costa Oliveira[1,2], Luís Guerra Rosa[2], Jorge Cruz Fernandes[2], José Rodríguez[3], Inmaculada Cañadas[3], Diego Martínez[3] and Nobumitsu Shohoji[1,*]

[1]*INETI-Instituto Nacional de Engenharia, Tecnologia e Inovação, I.P., DMTP-Departamento de Materiais e Tecnologias de Produção, 1649-038 Lisboa, Portugal*
[2]*IST-Instituto Superior Técnico, Departamento de Engenharia de Materiais, 1049-001 Lisboa, Portugal*
[3]*PSA-Plataforma Solar de Almería, CIEMAT-Centro de Investigaciones Energética, Medioambientales y Tecnológicas, P.O. Box 22, 04200 Tabernas Spain*

Consolidation of cordierite disc specimens was undertaken under concentrated solar beam in a solar furnace at PSA (Plataforma Solar de Almería). Satisfactory extent of densification was achieved by the present solar-sintering experiment. The mechanical properties measured for the solar-sintered cordierite test pieces were; density $\rho = 2.45 \pm 0.02\,\mathrm{g/cm^3}$, Vickers microhardness $HV = 7.31 \pm 0.29\,\mathrm{GPa}$, Young's modulus $E = 97 \pm 5\,\mathrm{GPa}$, shear modulus $G = 38 \pm 2\,\mathrm{GPa}$, Poisson ratio $\nu = 0.27 \pm 0.01$, fracture toughness $K_{IC} = 1.50 \pm 0.15\,\mathrm{MPa{\cdot}m^{1/2}}$ and modulus of rupture evaluated by ring-on-ring test $MOR_{ROR} = 57.8 \pm 13.7\,\mathrm{MPa}$ which were comparable to those of the counterparts sintered by conventional industrial gas furnace. [doi:10.2320/matertrans.MRA2008369]

(Received October 9, 2008; Accepted June 10, 2009; Published August 25, 2009)

Keywords: *cordierite, solar furnace, sintering, uniaxial flexure strength, equibiaxial flexure strength*

1. Introduction

Since its discovery in 1813, cordierite ($2MgO{\cdot}2Al_2O_3{\cdot}5SiO_2$), named after the French geologist Pierre-Louis-Antoine Cordier (1777-1861), has been the subject of extensive research. What makes cordierite most unique is its very low thermal expansion coefficient (as low as $7 \times 10^{-7}\,K^{-1}$ over temperature range 298–1273 K) and resultant excellent resistance to thermal shock ($\Delta T > 350\,K$).

Cordierite is widely used in glass ceramic compositions for manufacturing multilayer circuit boards, catalytic converters, diesel particulate filters, kiln furniture, thermal insulation parts, among others. Nowadays, most catalytic converters are commonly made from ceramics containing a large proportion of cordierite.[1)]

As reported earlier,[2)] a solar furnace (SF) at PSA (Plataforma Solar de Almería) was proved to be a convenient ecological heat source for synthesis of carbide and carbo-nitride of *d*-group transition elements (Ti, Zr, Hf; V, Nb, Ta; Cr, Mo, W). This SF at PSA is capable of heating test pieces located at a hot spot of diameter about 50 mm to 1873 K from ambient temperature within a few minutes.

However, use of SF as heat source for sintering of ceramic powder compacts was not always very successful on account of inherent technical problems associated with SF;
(a) certain extent of over-shoot of temperature at the onset of solar heating,
(b) difficulty in precise temperature control of the test piece.

For ceramic test piece that can be properly sintered only in relatively narrow window of temperature range (in case of cordierite, ±25 K around 1728 K[3)]), these technical demerits of SF would lead to either insufficient consolidation or over-sintering (undesired grain growth or partial melting). Anyway, we have attempted to use SF for sintering-consolidation of some ceramic powders[4–8)] and got to realise that following pragmatic cares must be taken towards realisation of acceptable solar-sintering of sample material.

The problems cited above as (a) and (b) are actually inter-related to each other. By uncontrolled over-shoot of temperature at the onset of the solar-heating test run, excessive proportion of liquid phase would emerge in the compacted powders to result in undesired geometrical distortion. On the other hand, if the achieved temperature by solar-heating is insufficiently low, satisfactory extent of sintering would not proceed. To avoid such lack in temperature control for sintering process, precise temperature monitoring is desirable. The precise temperature control in SF is quite difficult to realise. Non-contact radiation temperature measurement using optical pyrometer is not free from error related to calibration with emissivity. On the other hand, contacting temperature monitoring using thermocouple is not free from time-lag on account of heat capacity of the thermo-couple itself and protecting sheath.

Thus, as a compromising solution, we carried out preliminary temperature monitoring tests to determine the optimised temperature profiles to yield the optimum sintering temperature condition for the cordierite test piece.

The composition of the raw material powders used in this work was designed to yield fully dense cordierite consolidate under well controlled conventional gas firing at temperatures around 1573 K.

In our earlier attempt,[7)] we tried to sinter cordierite-based commercial ceramic powders, RP7 (porous cordierite-former; IEC group C520) and BL7 (dense cordierite-former; IEC group C410), using the SF at PSA. Unfortunately, the effort was not successful on account of the fact that the temperature achieved was not sufficiently high for sintering cordierite to full density. The cause leading to the failure of the solar-sintering in our earlier attempt was identified to be the lack of precise temperature control in the experimental

*Corresponding author, E-mail: nobumitsu.shohoji@ineti.pt

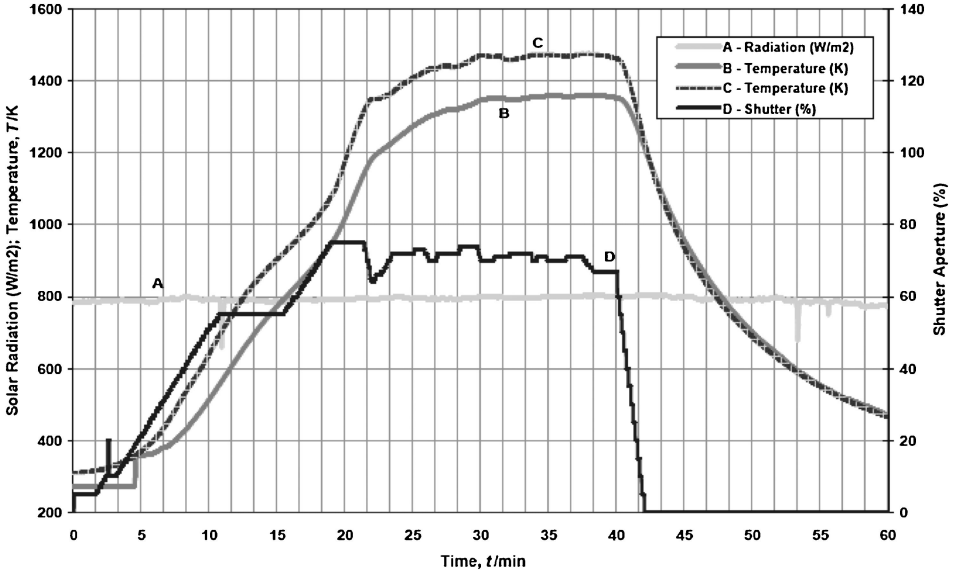

Fig. 1 Typical temperature monitoring results during a solar-sintering test run for cordierite.
curve A: solar energy density (W/m^2) measured with optical pyrheliometer at heliostat surface to ensure constancy of the received solar energy.
curve B: temperature (K) measured with a type B thermocouple placed at the centre of the alumina specimen holder beneath the test piece. This thermocouple was encased in alumina sheath.
curve C: temperature (K) measured with a type K thermocouple directly in contact with the centre of the test piece bottom surface. This thermocouple was used without sheath.
curve D: louvered shutter opening (%).

setting at that early stage of our experience with SF for sintering purpose.

However, in the more recent attempt of solar-sintering of alumina ceramics using SF at PSA,[8] it was verified that successful densification of alumina ceramic might be realised by carefully setting the solar-sintering conditions including gas environment and temperature. Alumina is an oxide ceramic and temperature window for sintering is not so narrow as the one for cordierite (±25 K).

Some of the authors (FACO & JCF) have been working also on consolidation of cordierite composites reinforced with zirconia (ZrO_2) and zircon ($ZrSiO_4$) through sintering in conventional laboratory electric furnace under well controlled thermal cycling conditions.[9–12]

2. Experimental

2.1 Specimen materials

The starting material was a commercial powder mixture of raw materials (including ball clays, talc, feldspar, alumina and silica) that forms cordierite upon firing at 1573 K in conventional gas furnaces. This powder mixture, supplied from Rauschert Portuguesa S.A., Carcavelos, Portugal, was characterised to be with a specific surface area = 11 $m^2 \cdot g^{-1}$, average particle size = 4.5 µm and true density = 2.91 $g \cdot cm^{-3}$.

The sequence of the chemical reactions that take place during firing, as depicted in typical DTA and TG curves together with XRD analysis, was described in detail elsewhere.[13]

Spray-dried granules were uniaxially pressed at 45 MPa to prepare test discs with diameter 30 mm and thickness 2.5 mm.

2.2 Sintering under irradiation of concentrated solar beam

Figure 1 shows the typical heating/cooling curves in the solar sintering processing. The temperature profiles measured using a type B thermocouple (curve B) and using a type K thermocouple (curve C) are presented in Fig. 1. All the measurements were carried out using an alumina sheath to avoid direct contact of the thermocouple with the solar radiation. Previous comparative test measurements using bare and sheathed thermocouples located in the vicinity of the solar beam central axis showed that, under steady state condition, the former showed a temperature by about 200 K higher than the latter although they were by no more than a few mm apart from each other. This is related to the white color of the alumina sheath (high reflectance) and the time-lag in the response to temperature change compared with that of the bare thermocouple. For this reason, after a few trial-and-error attempts, it was decided that the reading of the temperature-controlling sheathed thermocouple should not exceed 1473 K for realisation of adequate sintering without undesired melting of the cordierite disc specimen.

Initial tests were performed using the setup shown in Fig. 2 (left). Four discs were placed next to the thermocouple sheath located in the vicinity of the solar beam central axis. As can be seen, colour changes (being associated with different degrees of densification) were observed throughout the surface of the exposed discs. In addition, cracks were found to have propagated in some of the discs and considerable bending has occurred as well. It was therefore concluded that this setup under which the solar beam radiation was applied directly over the top surface of the compacted pellet of the sample powders was not appropriate for obtaining sintered cordierite bodies.

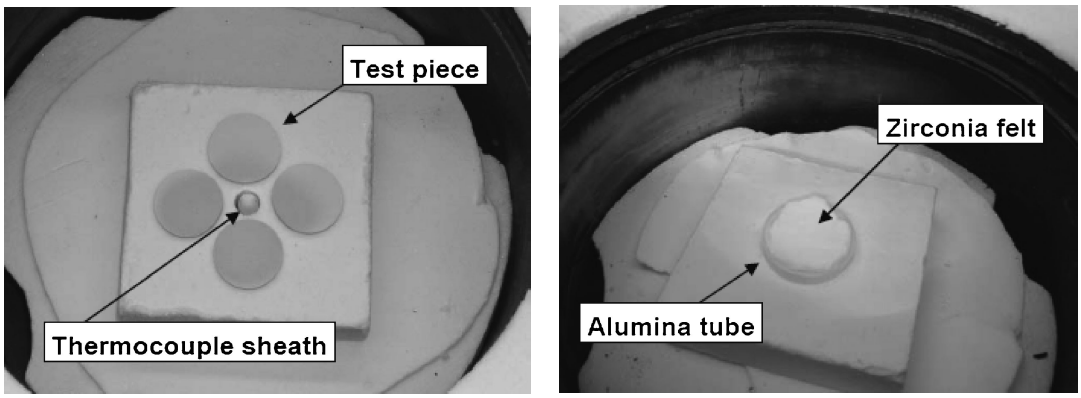

Fig. 2 Setups used to perform the sintering of cordierite discs experiments by direct exposure (left) and indirect exposure (right) to the solar radiation beam. As given in the text, the diameter of each disc test piece was 30 mm.

Thus, an alternative setup was arranged. A dense alumina tube was cut with a suitable thickness so that up to 4 discs could be piled up. The alumina sheath[14] was placed underneath the cordierite disc and centered with the solar beam. The alumina tube[15] was then covered with a zirconia (YSZ: yttria-stabilised zirconia) fiber mat in order to prevent the discs from being exposed directly to the solar radiation and to homogenise the temperature distribution for the piled-up 4 discs (Fig. 2, right). Using this setup, all discs could be sintered without any of the inconvenience described above experienced under the preliminary setup condition. Tests were then performed using more than one disc being piled up in a single run (2 discs or 4 discs). We managed to separate the discs from each other after the sintering under this setup. A temperature gradient was observed along the thickness of the tube[15] (no greater than 50 K along the height of about 15 mm) to result in the more glazed appearance for the sintered cordierite disc at the top than at the bottom. On the other hand, the area of the discs in touch with the thermocouple sheath was slightly lighter than elsewhere suggesting that densification was uneven as a result of the interaction between the two materials in close contact. For this reason, some of the MOR_{ROR} (modulus of rupture evaluated for disc specimen by ring-on-ring type equibiaxial flexure breaking test) data had to be discarded from the analysis (three test pieces, C, J and M3 in Table 1). These three test pieces excluded from the analysis yielded data points on the Weibull MOR_{ROR} plots deviated significantly away from the other 11 data points falling around a linear relationship. In fact, local surface appearances of these three excluded test pieces were different from the other 11 test pieces and broke up at comparatively low fracture loads; in terms of colour as well as of apparent high surface porosity. The detected localised colour change must be attributed to the chemical interaction between these test pieces and the thermocouple sheath. On the other hand, the apparent high surface porosity around the localised coloured zone appeared to indicate the insufficient extent of sintering progressed because of accidental contact of the thermocouple sheath with the test piece surface to have acted as a heat sink. As such, the measured low fracture stress levels for these three excluded specimens from the analysis must be largely ascribed to the localised high porosity level while additional contribution from the localised compositional modification cannot be ruled out (note that one of the constituents of cordierite is alumina). Levels of load F on fracturing for the test pieces, D (139.8 N) and H1 (133.6 N), were lower than that for the test piece C (141.3 N) but the test pieces, D and H1, were not excluded from the analysis.

Table 1 Parameter values measured for the 14 solar-sintered specimen discs with the 11 valid data used for the analysis being indicated with bold letters.

Specimen	h (mm)	$d = 2R_0$ (mm)	V (cm^3)	ρ (g/cm^3)	F (N)	MOR_{ROR} (MPa)
C*	1.78	27.56	1.06	2.43	141.3	32.94
D	**1.70**	**27.58**	**1.02**	**2.48**	**139.8**	**35.72**
H1	**1.50**	**27.72**	**0.91**	**2.41**	**133.6**	**43.79**
H2	**1.68**	**27.63**	**1.00**	**2.47**	**209.3**	**55.06**
J*	1.74	27.64	1.04	2.47	126.9	30.93
L	**1.90**	**27.78**	**1.15**	**2.45**	**211.5**	**43.18**
M1	**1.73**	**27.68**	**1.04**	**2.45**	**290.2**	**71.95**
M2	**1.92**	**27.57**	**1.15**	**2.43**	**285.9**	**57.28**
M3*	1.65	27.78	1.00	2.42	85.8	23.37
M4	**1.93**	**27.59**	**1.15**	**2.45**	**271.5**	**54.10**
N1	**1.46**	**27.78**	**0.88**	**2.43**	**155.4**	**54.10**
N2	**1.27**	**27.66**	**0.76**	**2.44**	**163.6**	**74.85**
N3	**1.25**	**27.49**	**0.74**	**2.45**	**155.1**	**73.96**
N4	**1.50**	**27.35**	**0.88**	**2.47**	**215.4**	**71.33**

h: test piece thickness,
d: test piece diameter,
R_0: the test piece radius,
V: test piece volume,
ρ: test piece density,
F: rupture load,
MOR_{ROR}: equibiaxial modulus of rupture determined by ring-on-ring test.

As already pointed out, consolidated bodies of polycrystalline cordierite ceramics with high strength, high density and low thermal expansion coefficient (TEC) of stoichiometric composition, $2MgO{\cdot}2Al_2O_3{\cdot}5SiO_2$, are difficult to manufacture because of the very narrow, impurity-sensitive firing range of this compound (±25 K around its incongruent melting point 1728 K[3]). Thus, it was quite an achievement to be able to sinter dense cordierite in SF at PSA under indirect solar exposure conditions.

Zeck and Williams[16] reported existence of the natural cordierite in the desert district of Almería near the solar furnace installation of the PSA where the present work was undertaken coincidentally. We believe that our present work would open up the way for a new path towards sintering-consolidation of this peculiar industrial ceramic.

2.3 Characterisation of mechanical properties for solar-consolidated cordierite disc

Bulk densities and open porosities of the sintered samples were determined by the Archimedes method, according to the IEC 672-2 standard.[17] The equibiaxial flexural strength tests were performed according to the procedure described in our earlier publication.[4] As a certain extent of bending (concentric deviation of top and bottom surface of the disk from flatness) was detected for all the solar-consolidated cordierite ceramic test pieces, the discs had to be hand-polished to obtain flat-surface test pieces to carry out valid self-aligning ring-on-ring (ROR) equibiaxial flexure fracture tests in an Instron machine using the setup shown in Fig. 2 in Ref. 4) The set of MOR_{ROR} data acquired under equibiaxial loading condition was analysed using the two-parameter Weibull statistics according to the ASTM C1239-06A.[18]

Dynamic Young's modulus E of sintered discs was determined using an acoustic measuring device (IMCE n.v.–Integrated Material Control Engineering, Diepenbeek, Belgium) known as the impulse excitation technique. In this method, the fundamental resonance frequency of flexural vibration of a sample is evaluated after it has been excited by a light mechanical impulse (tapping). The shear modulus G, the Young's modulus E and the Poisson's ratio ν were determined according to the procedure defined in the ASTM C1259-96.[19]

Value of Vickers micro hardness HV [N·m^{-2}] was calculated from the average length D [m] of the measured two diagonals in the base of the square indentation mark by

$$HV = 1.8544 \cdot P/D^2 \tag{1}$$

where P [N] refers to the indentation load (in this experiment, we used $P = 4.9$ N).

On the other hand, fracture toughness K_{IC} [MPa·m$^{1/2}$] was evaluated according to the indentation fracture method[20]

$$K_{IC} = 0.018 \cdot (E/HV)^{1/2} \cdot (P/c^{3/2}) \tag{2}$$

where c [m] refers to the half length of the cracking flaw introduced by the Vickers indentation as depicted in Fig. 3. Equation (2) was used for the calculation of K_{IC} because the emerged crack around the Vickers indentation mark for the solar-sintered cordierite test piece was identified to be the median/half-penny flaw as depicted in Fig. 3 rather than the radian/Palmqvist type.

On the other hand, MOR_{ROR} values under the equibiaxial loading condition were calculated using a formula[4,6]

$$MOR_{ROR} = [3F/(2\pi h^2)] \cdot [(1+\nu) \cdot \ln(R_2/R_1) + (1-\nu) \cdot (R_2{}^2 - R_1{}^2)/(2R_0{}^2)] \tag{3}$$

where F refers to the rupture load, h the disc specimen thickness, ν the Poisson's ratio, R_1 the inner (upper) ring radius (3.8 mm) of the ROR test jig, R_2 the outer (lower) ring radius (11 mm) and R_0 the disc specimen radius.

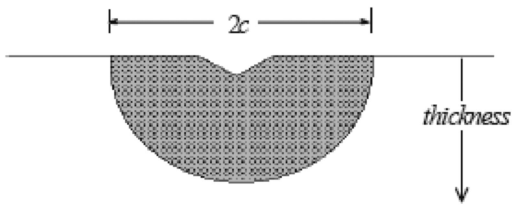

Fig. 3 Schematic cross section of the median/half-penny type flaw developed around a Vickers indentation mark showing definition of $2c$ (length of the cracking flaw).

3. Results and Discussion

3.1 Mechanical properties of the solar-sintered cordierite disc specimens

Table 1 lists the measured properties of the 14 solar-sintered cordierite discs together with the calculated values of test piece volume V (cm^3), density ρ (g·cm^{-3}) and MOR_{ROR} (MPa). The HV measurements were made for the four test pieces, N1-N4. The HV value was calculated to be 7.31 ± 0.29 GPa from the total 40 measurements (10 measurements for each test piece) using eq. (1). All the other parameter values were measured for all the 14 test pieces but the average was made over the 11 valid test pieces by excluding the results for the 3 test pieces that yielded the MOR_{ROR} values out of contention (Table 1). As pointed out earlier in the text towards the end of **2.2**, appearances of these three text pieces, C, H1 and M3, were evidently distinguishable from those of the others and we suspected that the possible cause for this was the interaction of those test pieces with the thermocouple sheath made of alumina leading to introduction of surface porosity and consequent loss of strength F on fracturing. Density ρ was evaluated to be 2.45 ± 0.02 g·cm^{-3}, Young's modulus $E = 97 \pm 5$ GPa and shear modulus $G = 38 \pm 2$ GPa. From the measured values for E and G, Poisson's ratio ν was calculated to be $\nu = 0.27 \pm 0.01$ under assumption of the test piece isotropy using the relation

$$\nu = (E/2G) - 1 \tag{4}$$

Then, fracture toughness K_{IC} was calculated using the measured values of E and HV according to eq. (2) to be 1.50 ± 0.15 MPa·m$^{1/2}$ and MOR_{ROR} on the basis of eq. (3) to be 57.8 ± 13.7 MPa. When the MOR_{ROR} was calculated for all the 14 test pieces, it yielded the mean value 51.6 MPa in place of 57.8 MPa with a slightly greater extent of scatter ($\pm$17.2 MPa in place of $\pm$13.7 MPa).

3.2 Mechanical properties of the cordierite disc specimens consolidated by conventional industrial sintering route

For comparison purposes, 21 discs of industrial dense cordierite were prepared by uniaxially pressing at 45 MPa and then sintered in an industrial gas furnace at Rauschert Portuguesa, S.A. Table 2 summarises the MOR_{ROR} values calculated according to eq. (3) for these comparative test pieces.

From the data summarised in Table 1 and 2, the arithmetic mean MOR_{ROR} value ($\pm$ standard deviation) as well as the unbiased estimated m and σ_0 values-determined according

Table 2 Equibiaxial fracture strength values of the dense cordierite disc specimens sintered in the conventional industrial gas furnace.

Specimen	h (mm)	d (mm)	F (N)	MOR_{ROR} (MPa)
1	3.35	27.75	882.1	57.65
2	3.30	27.73	894.2	60.24
3	3.28	27.79	618.0	42.12
4	3.37	27.73	805.9	52.06
5	3.40	27.77	853.7	54.16
6	3.30	27.74	896.4	60.38
7	3.31	27.78	692.9	46.37
8	3.34	27.75	954.6	62.76
9	3.23	27.75	963.5	67.74
10	3.28	27.75	878.9	59.92
11	3.31	27.75	774.0	51.82
12	3.31	27.76	936.8	62.71
13	3.29	27.76	687.8	46.60
14	3.29	27.74	764.6	51.82
15	3.26	27.76	768.1	53.01
16	3.33	27.75	872.5	57.71
17	3.30	27.75	839.7	56.56
18	3.30	27.75	700.4	47.17
19	3.28	27.75	687.5	46.87
20	3.15	27.75	873.6	64.58
21	3.25	27.75	797.6	55.85

to ASTM C1239-06A[18] -together with their upper (95%) and lower (5%) bonds were evaluated and listed comparatively in Table 3.

Other characteristics of the conventionally-sintered discs were also determined: bulk density $\rho = 2.36 \pm 0.01\,\mathrm{g{\cdot}cm^{-3}}$; $E = 89.0 \pm 1.4\,\mathrm{GPa}$; $G = 35.7 \pm 0.8\,\mathrm{GPa}$; $\nu = 0.27 \pm 0.01$.

3.3 Weibull statistical analysis

Conventional mechanical integrity assessment involves testing of a relatively small number of test pieces, generally at least five. Under these conditions, a mean nominal fracture strength can be calculated but the figure may not be reliable. It might be used as a quality control purpose but should not be used for stress calculations.

Because the failure under consideration occurred at a critical flaw, it can be described by the weakest link theory. A probability function that describes the strength distribution of brittle materials is acknowledged to be the Weibull function. The set of flexural strength data might therefore be analysed on the basis of the two-parameter Weibull distribution model in terms of *shape* parameter m and *scale* parameter σ_0. However, only in case of a large number of test pieces being available, say 20 or more, the best fit to the strength data distribution is achieved using the Weibull distribution. The shape parameter m is also known as the Weibull modulus and considered as a measure of the scatter of strengths obtained; the higher the m value the smaller the extent of the scatter of the MOR_{ROR} data.

On the other hand, the *scale* parameter determines the range of the distribution. For the MOR_{ROR} data under consideration, the *scale* parameter corresponds to the characteristic strength σ_0. That is, 63.2% of all the MOR_{ROR} values fall in the range smaller than the characteristic strength σ_0.

Validity of the Weibull approach is guaranteed only when the analysis is made for a relatively large number of data. However, the acquired number of test pieces available from experiments performed under the present solar sintering conditions was mere 11. On account of this reality, we decided to undertake estimations for the Weibull modulus m (shape parameter) and the characteristic strength σ_0 (scale parameter) according to the Maximum Likelihood technique following the ASTM C1239-06A standard[18] with unbiasing factors along with 95% confidence bounds about both parameters assuming that a single-flaw population alone was active as confirmed by the fractography.

The effect of sintering conditions on MOR_{ROR} is compared in Table 3 in terms of m and σ_0. It may be inferred that mean MOR_{ROR} values are comparable to each other between the solar-sintered and the conventionally-sintered test pieces within the experimental error of the measurements and the size of populations. It is also not surprising that the estimates of m increase with the increasing number of the test pieces (i.e. the m determined for the solar-sintered test pieces was smaller than that for the conventionally-sintered counterparts). Obviously, temperature control is tighter in the case of conventional gas furnace sintering than in the solar sintering. We noticed that the discs sintered in the solar furnace were slightly glazed. This is an indication that the processing temperatures in the solar-sintering experiments must have exceeded typical conventional sintering temperature 1573 K and thence the amount of glass phase pockets present in the microstructure have also increased as might be noticed in the optical micrographs (Fig. 4). As a result, the material should behave in a more fragile fashion and it is not therefore surprising that m dropped by half, from *ca.* 9 for the conventionally-sintered test pieces to 4.5 for the solar-sintered counterparts. One should also bear in mind that the solar-sintered discs were obtained from different batches of solar irradiation test runs (Table 1) whereas all the conventionally-sintered dense cordierite test pieces were prepared together by a single batch of firing run (Table 2). Therefore, this might also have influenced the extent of scatter of the data together with the inherent difficulty in the precise temperature control in the solar-sintering operation.

Table 3 Mechanical properties of the solar-sintered and the conventionally-sintered cordierite discs. Weibull parameters, m and σ_0, were calculated according to Ref. 18) using maximum likelihood estimators.

Treatment designation	MOR [MPa]	Weibull modulus m	characteristic strength σ_0	HV [GPa]	K_{IC} [MN·m$^{-3/2}$]
Solar sintering	57.8 ± 13.7	$4.5^{7.0}_{3.0}$	$63.0^{70.8}_{55.9}$	7.31 ± 0.29	1.50 ± 0.15
Conventional sintering	55.2 ± 6.9	$8.7^{11.8}_{6.4}$	$58.1^{60.8}_{55.5}$	7.58 ± 0.56	1.10 ± 0.24

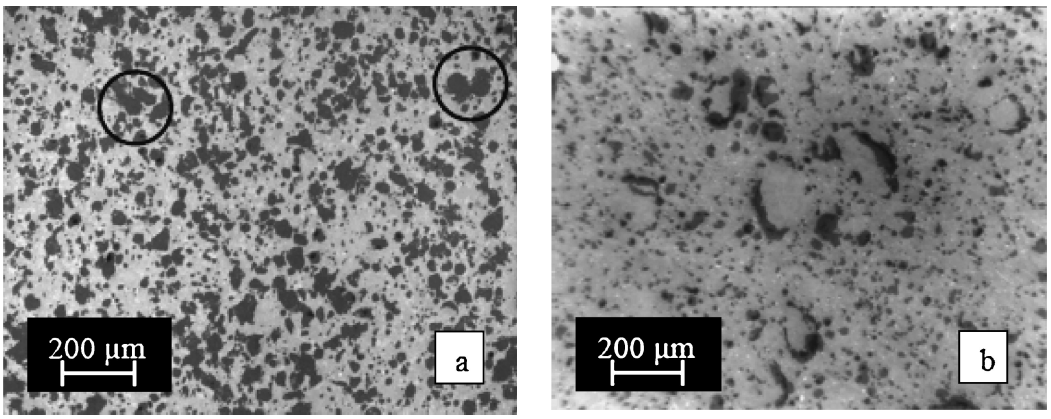

Fig. 4 Optical micrographs of polished cross-sections of discs sintered for 30 min in (a) conventional gas furnace, (b) solar furnace. The circles in the picture (a) indicate coalescence of glass pocket regions.

Note also that the relatively large confidence bounds associated with this estimation of m is mainly related to the smaller size of the solar-sintered test pieces population when compared to the conventionally-sintered ones. Nevertheless, from a statistical viewpoint, the MOR_{ROR} values fall within the same interval taking into account the error margin of the statistical estimate. Therefore, one may conclude that, within the limitations of temperature control and small number of available solar-sintered test pieces, cordierite discs with properties comparable to those of the conventionally-sintered counterpart might be obtained through ecological solar radiation-sintering within incomparably shorter heating cycle (about 60 min including heating and cooling durations before and after the 30 min solar irradiation) compared to the conventional process (around 24 h). This is certainly a major advantage of the solar-sintering as a novel industrial production technology.

3.4 Comparison of the equibiaxial strength with the uniaxial bending strength

Equibiaxial strengths and four-point bending strengths can not be directly compared. A multiaxial stress state exists in equibiaxial flexure testing and the calculation of the effective area is more complex than in the case of uniaxial flexure testing (e.g. 4-point bending test) since an assumption regarding the effect of a multiaxial fracture criterion must be considered. By using the Weibull statistics, however, the concerned differences can be accounted for and prediction of the data to be acquired under equibiaxial stress condition from the data acquired under multiaxial stress state or *vice versa* might become feasible. Batdorf[21] and Breder *et al.*[22] reviewed this problem for the fixture geometry used in the present study and drew the following relationship for the effective area $A_{eff(ROR)}$ (mm^2) for the ring-on-ring type equibiaxially tested specimen:

$$A_{eff(ROR)} = 2\pi \cdot {R_1}^2 \cdot m^{0.45} = 90.7m^{0.45} \quad (5)$$

where R_1 refers to the radius of the upper loading ring (3.8 mm in this study). Since $m = 8.7$ (Table 3), value for the $A_{eff(ROR)}$ is calculated to be 240 mm^2.

In the case of uniaxial flexural test, the effective area $A_{eff(UFS)}$ (mm^2) for 4-point bending test piece is calculated by[23]

$$A_{eff(UFS)} = A \cdot [b \cdot m/(b+h) + 1] \cdot [(L_I/L_O) \cdot m + 1]/(m+1)^2 \quad (6)$$

where A refers to the test piece surface area under tension, b the specimen width (4 mm), h the thickness or height (3 mm), L_I the inner loading span (20 mm) and L_O the outer loading span (40 mm). The area A is calculated by

$$A = L_I \cdot (b+h) \quad (7)$$

By substituting m with 16.3 determined for the UFS (uniaxial flexure strength) type test piece of the consolidated dense cordierite by sintering in industrial gas furnace (cf. Table 5 in Ref. 12)), $A_{eff(UFS)}$ is calculated by eq. (6) to be 44 mm^2.

Assuming the maximum stress being equal to the fracture strength and the strength-limiting surface flaw being comparable to one another, the failure stresses of the two distinguishable specimen geometries may be related by

$$\frac{MOR_{UFS}}{MOR_{ROR}} = \left[\frac{A_{eff(ROR)}}{A_{eff(UFS)}}\right]^{1/m} \quad (8)$$

where the suffix "UFS" stands for the *uniaxial flexure strength* and "ROR" the *ring-on-ring equibiaxial flexure strength*. Provided that the evaluated value for the strength was controlled by volume flaws, eq. (8) would not be valid. The value for m was determined to be 16.3 in the case of conventionally-sintered dense cordierite samples tested under uniaxial flexure test conditions[12] while m in the case of equibiaxial testing was evaluated to be 8.7 as presented in Table 3. The difference in m might be related to the fact that the effective area in equibiaxial testing is about 5.5 times greater than that under uniaxial testing. Assuming that $m = 9$ (on the basis of $m = 8.7$ for the conventionally-sintered dense cordierite test piece given in Table 3), one obtains $MOR_{UTS} = 1.21\ MOR_{ROR}$ from eq. (8) meaning that the value estimated (66.6 MPa) is (probably by coincidence) comparable to the experimental value 67 MPa in our earlier work for the same dense cordierite composition.[12]

It may therefore be inferred that the equibiaxial flexure strengths (55.2 ± 6.9 MPa) were by about 20% less than the uniaxial flexure strength (67 ± 5 MPa[12]). This amount correlates very well with the predicted strength-size scaling between the two geometries using Weibull statistics and

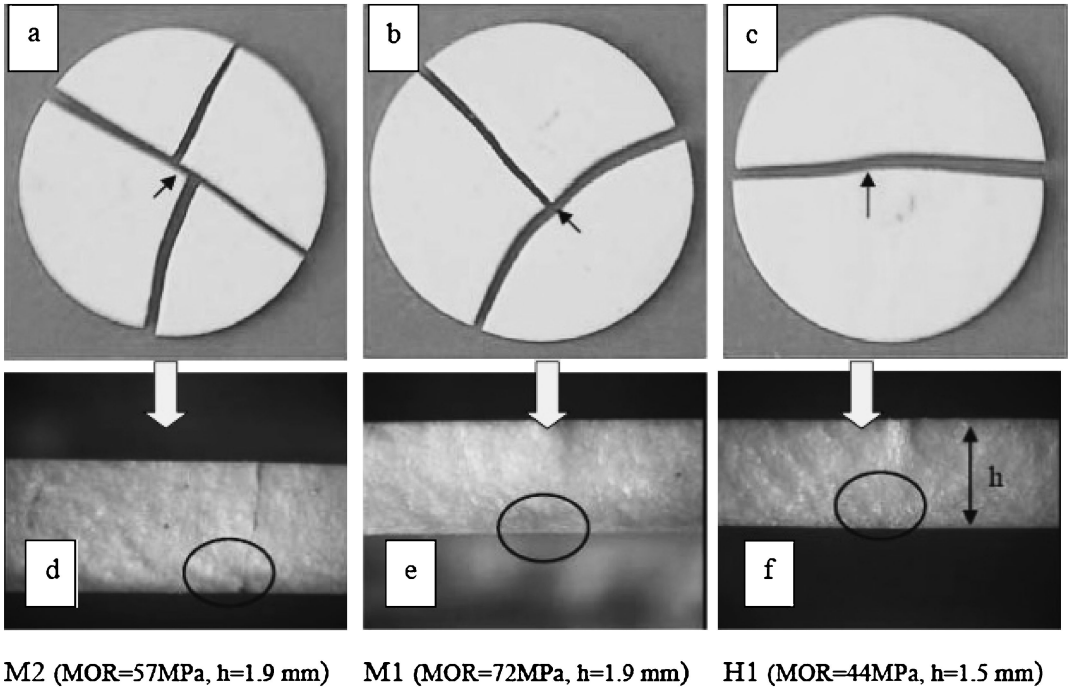

Fig. 5 Typical low strength crack patterns of solar-sintered cordierite discs (denoted as (a), (b) and (c)) together with cross-sectional fractographic stereo microscopy images showing the primary fracture initiation location ((d), (e) and (f), respectively) as indicated by the black circles. As given in the text, the diameter of each disc test piece was 30 mm.

eq. (8). Because the equibiaxial flexure strength is lower and probably more representative of the on-center loading of ceramic tiles, its use is conservative and probably better suited than the use of uniaxial flexure strength for input in models that consider such deflections (e.g. armor tiles ballistic modeling).

3.5 Fractography

It is well established that the size of the critical origin defect, a (i.e. depth of a flaw) can be estimated using the Griffith's equation according to:

$$a = \left[\frac{K_{\mathrm{Ic}}}{MOR \cdot Y}\right]^2 \tag{9}$$

where Y refers to the stress intensity shape factor for the origin depending on the crack geometry ($Y = 1.99$ when $c^* \gg a^*$, where c^* and a^*, respectively, are the length and the width of the defect).[24] Taking into account the values of MOR_{ROR} and K_{IC} listed in Table 3, one obtains the a values ranging from 100 to 183 μm, depending upon the treatment conditions. This is in good accord with the observations made by fractography (Fig. 5). Typical fracture defects and crack patterns shown in Fig. 5 indicate that all tests were valid (i.e. the fixture did not cause the fracture event) and the arrows pointing at the starting spots of the surface fracturing. Indeed, most origins of cracks appeared to be surface-related and the size of the critical defect is in agreement with the observations made on a Wild M8 Heerbrugg stereomicroscope (Switzerland). In addition, observations made on a Zeiss Axiovert 200 (M-7) microscope (Germany) revealed that the microstructure of cordierite sintered under solar radiation differs from that obtained by the conventional sintering. As already pointed out earlier in the text, the volume fraction of the glassy phase present was higher in the former than in the latter (Fig. 4), which explains rationally the observed evidence that the degree of the densification achieved was higher for the former than the latter. Hence, slightly higher values of ρ, E, G, HV and K_{IC} were obtained for the solar-sintered discs than those for the conventionally-sintered ones. The comparatively large size of the defects responsible for the failure initiation of the solar-sintered discs was likely to be related to coalescence of some pockets of glass phase, as highlighted in Fig. 4.

4. Concluding Remarks

We managed to consolidate cordierite ceramic disc test pieces by solar-sintering overcoming technical difficulties including the inherent temperature gradient along the height in the solar furnace and the narrow temperature window for optimised sintering (±25 K) through pragmatic modifications of the experimental setup. The solar-sintered cordierite disc specimens possessed mechanical properties comparable to those of the counterparts prepared by conventional laboratory or industrial process or to those of the cordierite-zirconia or cordierite-zircon composites.[9–11]

Much reduced processing duration (about 60 min) compared with that under the conventional processing (typically 24 h) is considered to be one of major advantages in view of industrial productivity besides ecological aspect of using renewable energy in view of diminished CO_2 emission.

Acknowledgements

The authors are grateful to Mr. Richard Palmeiro and Mr. Diamantino Dias at Rauschert Portuguesa S.A. for carrying

out the conventional gas furnace sintering for the reference dense cordierite specimen described in the section 3.2, to Mr. Paulino Verdasca at INETI for experimental determination of HV and K_{IC} and also to Ms Vera Pires (a post-graduate student at IST) for undertaking the Weibull statistical analysis of the data.

REFERENCES

1) A. Okada: J. Euro. Ceram. Soc. **28** (2008) 1097–1104.
2) J. Rodriguez, D. Martinez, L. Guerra Rosa, J. Cruz Fernandes, P. M. Amaral and N. Shohoji: J. Solar Energy Engineering (Trans. ASME) **123** (2001) 109–116.
3) R. Morrell: Proc. Brit. Ceram. Soc. **28** (1979) 53–71.
4) J. Cruz Fernandes, P. M. Amaral, L. Guerra Rosa and N. Shohoji: Ceram. Internat. **26** (2000) 203–206.
5) L. Guerra Rosa, P. M. Amaral, C. Anjinho, J. Cruz Fernandes and N. Shohoji: Ceram. Internat. **28** (2002) 345–348.
6) P. M. Amaral, C. Anjinho, J. Cruz Fernandes, L. Guerra Rosa and N. Shohoji: Proc. 8th Portuguese Conf. on Fracture, Sociedade Portuguesa de Materiais, (Vila Real, February 2002), pp. 395–399.
7) F. Almeida Costa Oliveira, N. Shohoji, J. Cruz Fernandes and L. Guerra Rosa: Solar Energy **78** (2005) 351–361. DOI: 10.1016/j.solener.2004.08.013
8) R. Román, I. Cañadas, J. Rodrígues, M. T. Hernández and M. González: Solar Energy **82** (2008) 893–902. DOI: 10.1016/j.solener.2008.04.002
9) F. Almeida Costa Oliveira and J. Cruz Fernandes: Ceram. Internat. **28** (2002) 79–91.
10) F. Almeida Costa Oliveira, J. A. Franco and J. Cruz Fernandes: Key Eng. Mater. **206–213** (2002) 1029–1032.
11) F. Almeida Costa Oliveira, J. A. Franco and J. Cruz Fernandes: Key Eng. Mater. **230–232** (2002) 84–87.
12) F. Almeida Costa Oliveira, J. A. Franco, J. Cruz Fernandes and D. Dias: Brit. Ceram. Trans. **101** (2002) 1–8.
13) M. J. Matos, S. Dias, F. Almeida Costa Oliveira: Adv. Appl. Ceram.: Structural, Functional and Bioceramics **106** (2007) 209–215.
14) The "alumina sheath" refers to the one-end-closed tube protecting the thermocouple.
15) On the other hand, the "alumina tube" refers to the open tube used as the sample container.
16) H. P. Zeck and I. S. Williams: J. Petrology **43** (2002) 1089–1104.
17) IEC Standard Publication 672-2, Specification for Ceramic and Glass Insulating Materials Part 2: Methods of Test, First Edition, (Bureau Central de la Commission Electrotechnique Internationale, Genève, Switzerland, 1980).
18) ASTM C1239-06A: Standard Practice for Reporting Uniaxial Strength Data and Estimating Weibull Distribution Parameters for Advanced Ceramics, (2007).
19) ASTM C1259-96: Standard Test Method for Dynamic Young's Modulus, Shear Modulus and Poisson's Ratio for Advanced Ceramics by Impulse Excitation of Vibration, (1996).
20) JIS R 1607, Testing Methods for Fracture Toughness Methods of High Performance Ceramics, (1990).
21) S. B. Batdorf: Internat. J. Fracture **13** (1977) 5–11.
22) K. Breder, T. Andersson and K. Schölin: J. Am. Ceram. Soc. **73** (1990) 2128–2130.
23) N. A. Weil and I. M. Daniel: J. Am. Ceram. Soc. **47** (1964) 268–274.
24) ASTM C1322-05B: Standard Practice for Fractography and Characterization of Fracture Origins in Advanced Ceramics, (2007).